The Analyzing Power of the Positron Polarimeter of E166

DESY Zeuthen Summer Student Program

Final Report

Richard I. Anderson

September 13, 2006

Abstract

As a Summer Student at DESY Zeuthen from July 26, 2006 till September 19, 2006, I was part of the Linear Collider group. The goal of my work was to determine the analyzing power, A_γ, of the positron polarimeter of the E166 experiment conducted at SLAC [1].
In this article, I will explain my work, starting with an overview of the E166 experiment as an introduction.

Topics of this paper include: The E166 experiment, the undulator-based method of producing polarized positrons, the degree of polarization of a particle beam, pair production, Bremsstrahlung, annihilation, transmission of radiation through a solid, cross-sections for Compton-Scattering, Geant4 simulations including polarized processes and, most importantly, the analyzing power.

Contents

Part I
Introduction

As an introduction to my work, I would like to give an overview of its importance. I will explain the E166 experiment, its importance for the ILC and explain the main goal of my work, the analyzing power. In *part II*, I will continue to report on what I did, explaining fundamental physical processes, such as polarization in Geant4 and finally present my results for the analyzing power.

1 The E166 Experiment

The E166 experiment is a demonstration experiment conducted to prove that polarized positrons can be produced using the undulator-based method.
Its two goals were

1. to produce polarized positrons and
2. to measure their degree of polarization.

Since both a highly polarized electron and positron beam are desired in the ILC, E166 is a very important experiment. It investigates a new technique of creating polarized positrons that would make use of the undulator, which is already part of the current baseline configuration of the ILC.
Together with the highly polarized electron beam, cross-sections for certain interactions can be modified. Using polarization, the signal-to-noise ratio for certain interactions could be enhanced considerably and the detection of the Higgs particle, if it exists, made clearer and easier.

1.1 The Undulator-Based Method

A beam of electrons is sent through a helical magnetic field in an undulator. This magnetic field effects the motion of the electrons and accelerates them transversely. Since accelerated electrons emit Synchrotron Radiation and since the direction of the motion is mapped on the direction of polarization of the emitted photons, circularly polarized Synchrotron Radiation emerges from the undulator.
After travelling for about 30m, the photon beam is collimated using a Tungsten collimator and is then incident on a photon target behind a lead wall. In the photon target, both electrons and positrons are produced due to pair production. Polarization is conserved for the emerging pair-produced particles. Polarization for charged particles refers to their spin direction. Behind the photon target is a solenoid used to focus the beam.

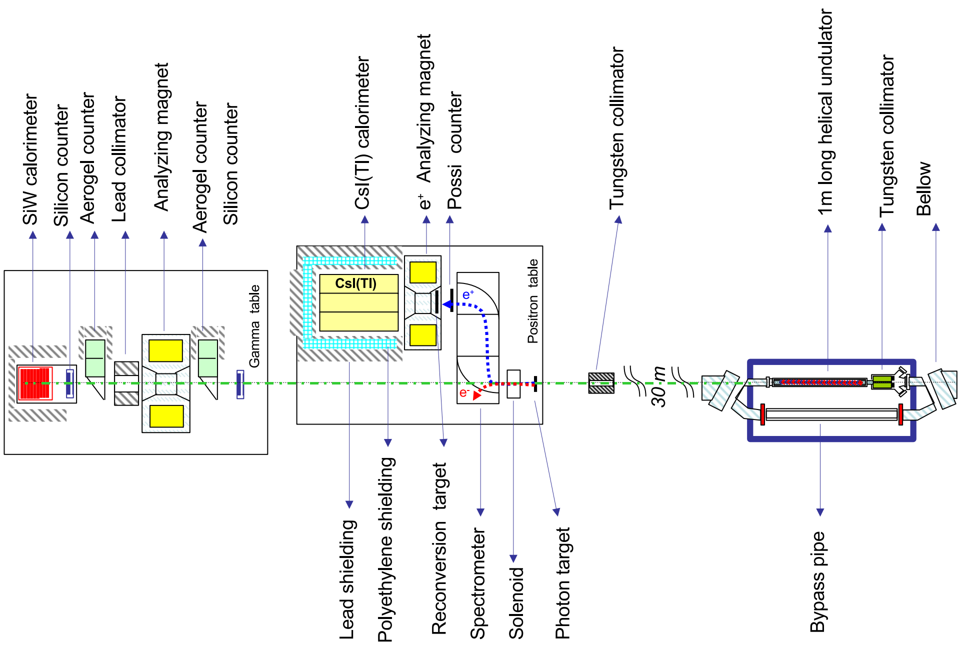

Figure 1: Provides a schematic overview of the E166 experiment. From right to left: Undulator-based source, photon target, solenoid, spectrometer, positron polarimeter and photon polarimeter, respectively

Using a Spectrometer, all three types of particles, namely e^-, e^+ and γ, are separated and only a certain energy range is selected for the positrons, while the electron-beam is dumped. The photons continue traveling straight ahead into the photon polarimeter which will not be discussed here. The beam of polarized positrons coming out of the spectrometer already consitutues Goal One of the experiment.
Goal Two now is to find the degree of polarization of this beam and thus showing that the undulator-based method for producing polarized positrons works.

1.2 The Positron Polarimeter

The polarimeter consisted of three main parts:

- A Tungsten reconversion target (RT) used for reconverting the incoming positron beam into photons via Bremsstrahlung and annihilation
- An analyzing magnet for changing the polarization of its iron core and thus changing the cross-section for Compton-Scattering, i.e. the energy transmitted through the iron to the calorimeter and

- The CsI calorimeter used to measure the asymmetries.

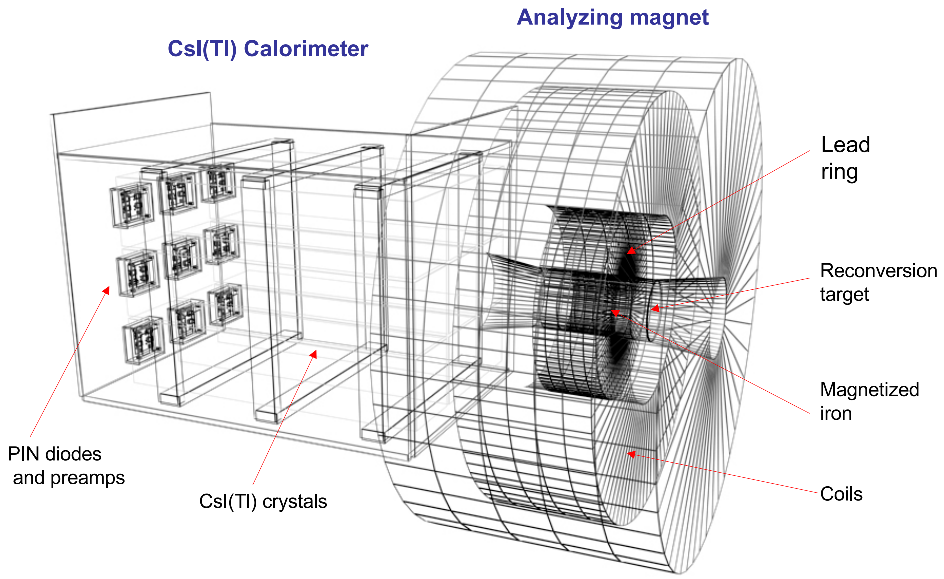

Figure 2: Shows the schematic setup of the polarimeter

For different directions of the magnetic field inside the analyzing magnet, hence different directions of polarizations, asymmetries in transmitted energy were measured. The asymmetry can be calculated according to the below formula:

$$\delta = \frac{E^+ - E^-}{E^+ + E^-} \tag{1}$$

E^+ stands for the '+' direction of polarization in the iron, E^- for the other. These definitions become clearer when looking at the analytical formula for the transmission of photons through a solid. Note the last exponential term incorporating the degree of polarization of the iron core.

$$E(L) = e^{-nL(\sigma_{phot}+\sigma_{pair}+\sigma^0_{comp})} e^{\pm nLP_\gamma P_e \sigma_{pol}} \tag{2}$$

Here, L is the length of the iron core inside the analyzing magnet, n the amount of scattering events, σ_{phot} the cross-section for the photo-electric effect, σ_{pair} the cross-section for pair production, σ^0_{comp} the one for unpolarized Compton-Scattering and σ_{pol} the cross-section for Compton-Scattering of polarized particles. From inserting the respective formulations for $E(L)$ into the equation for the Asymmetry, one can approximate that only P_e affects the Asymmetry, since everything else can be approximated to cancel out.

1.3 The Analyzing Power

It is imparative to know the analyzing power when determining the degree of polarization of the incoming positron beam. As can be seen from equation 3, the degree of Polarization P_γ of the photons emerging from the reconversion target P_γ translates to P_{e^+}, the degree of polarization of the positrons.

$$P_\gamma = \frac{\delta}{A_\gamma P_e} \tag{3}$$

However, the analyzing power cannot be determined experimentally. It must be obtained from Monte Carlo, in this case: Geant4 simulations.

Part II

What I did

2 Fundamental Physical Processes

2.1 General Remarks on this Section

In order to get an understanding and feeling for how Geant4 simulates physical processes, I started my work by running simplified simulations. I investigated the transmission probability through iron compared to that of vacuum, the contribution to photon energy from annihilation for positrons and the difference of energy contribution from Bremsstrahlung for electrons and positrons incident on the reconversion target (RT). In these, no magnetic field was applied inside the analyzing magnet; let me therefore call these simulations 'unpolarized'. First, a so-called pencil beam, i.e. an infinitesimally thin beam directed along the z-axis of the system, was used. With these starting conditions, I could pay particular attention to the individual physical processes present.
For these considerations, I used the E166polarimeter program written by Karim Laihem and the following statistics for both electrons and positrons:

- 1 Particle per bunch, 10000 bunches
- 100 Particles per bunch, 1000 bunches
- 1000 Particles per bunch, 1000 bunches

It soon became evident that low statistics give little information about this particular setup, due to the rather low probability of transmission through the iron core. This is especially true for single-particle bunches.

2.2 Transmission Probability through the Core

Transmission coefficients for iron are well-known. From the NIST homepage [5], a tabulated value of $\frac{\mu}{\rho} = 3.146 \times 10^{-02} \frac{cm^2}{g}$ was found for a photon beam energy of 5 MeV.
Since in my case the simulation was run with a positron beam energy of 5 MeV incident on a reconversion target, the energy detected by the calorimeter was an energy distribution in the range of 1 to 5 MeV due to the continuous loss of energy from Bremsstrahlung in the RT.
In our case we have a 7.5-cm-thick iron cylinder which is 2.5 cm in radius. With this geometry, and the formula for mass extinction

$$\frac{\langle E_{Fe} \rangle}{\langle E_{Vac} \rangle} = e^{-\frac{\mu}{\rho} \cdot x}$$

$\langle E_{Fe} \rangle$ (MeV)	Error	$\langle E_{Vac} \rangle$ (MeV)	Error	Figure
8.6	3.1×10^{-1}	8.2×10^{1}	7.2×10^{-1}	3

Table 1: Energies obtained for 1000 positrons per bunch and 1000 bunches. MeV

$$ \tag{4}$$

I calculated the mass attenuation coefficient $\frac{\mu}{\rho}$ from the mean energy arriving at the calorimeter and the formula

$$(7.5cm \cdot \rho)^{-1} \cdot \ln \frac{\langle E_{Fe} \rangle}{\langle E_{Vac} \rangle} = \frac{\mu}{\rho} \tag{5}$$

using the known density of iron: $\rho_{Fe} = 7.9 \frac{g}{cm^3}$. Here, $\langle E_{Vac} \rangle$ is the mean energy for vacuum, $\langle E_{Fe} \rangle$ the one for transmission through iron, x is the mass thickness defined by the thickness of the material multiplied by its density. Table 1 shows the mean energy values obtained by fitting the interpolated data for the whole calorimeter. Using the above procedure and the values from Table 1, a value of

$$\frac{\mu}{\rho} \approx 3.8 \times 10^{-2} \frac{cm^2}{g}$$

was obtained. Remembering that not all photons travel along the z-axis, as e.g. for an monoenergetic photon beam, and thus have to pass through more than 7.5cm of iron and also considering the error of the mean energy from the fit, this result can be considered in good accordance with the tabulated value. The form of the distribution of photon energy after reconversion plays an important role here. It will be broadened even more by annihilation radiation, since we are using positrons.
In order to make more precise statements on the transmission probability, higher statistics should be used. For further analysis, a comparison with an x-ray beam and vacuum in the Geant4-geometry of the reconversion target could be useful.

The Mean Energy of Photons in the Calorimeter: In order to find out the mean energy needed for photons to pass through the iron core, I compared values obtained for very high statistics at 1 positron per bunch and 1,000,000 bunches for a 'vacuum' core, i.e. vacuum chosen as the material inside the core of the analyzing magnet, and an iron core. As expected,

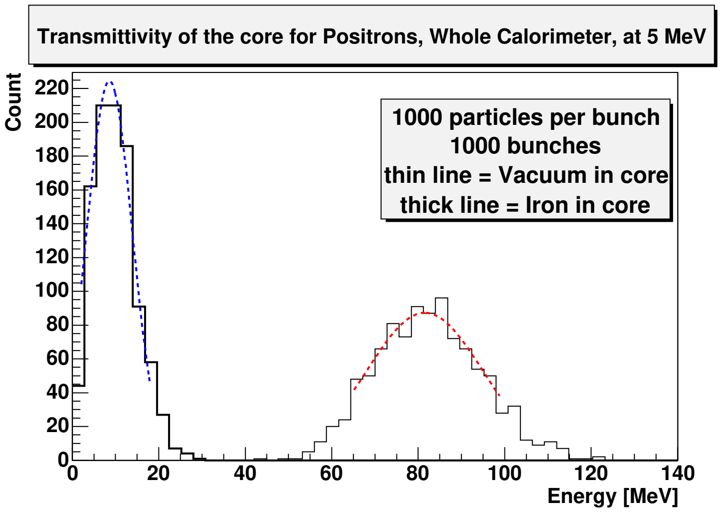

Figure 3: Shows the absorption of energy from the iron core by comparing those arriving at the calorimeter for iron and vacuum inside the core respectively. The values for the mean energies used to calculate the mass attenuation coefficient were obtained from the Gaussian fits.

$\langle E_{Fe} \rangle$	Error	$\langle E_{Vac} \rangle$	Error	Figure
2.11	± 0.0158	1.56	± 0.00446	4

Table 2: Mean energies of the positrons when comparing vacuum with iron as the core material in the analyzing magnet. 1,000,000 bunches with 1 particle each. Energies and errors in MeV.

the mean energy for an iron core turned out to be higher than for vacuum, cf. Table 2, since the transmission probability through a solid is energy-dependent.

In addition, Figure 4 shows an energy-weighted diagram for the energy deposited in the calorimeter. One can see clearly that even more than factor of 10 more particles are found in the central crystal in the case of vacuum compared to iron in the core. This explains why, for vacuum, a higher total energy is detected in the calorimeter while the mean energy per particle is lower. It is important to note that the maximum energy of the photons exceeds 5 MeV due to in-flight annihilation of an incoming positron with an electron at rest inside the reconversion target.

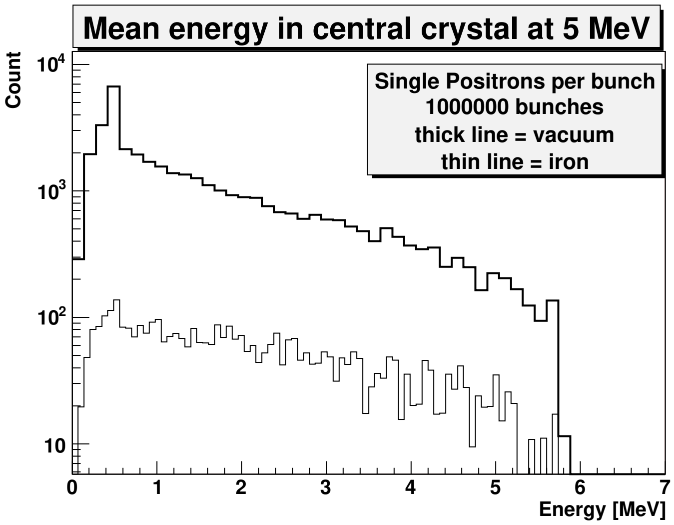

Figure 4: Mean energy of a photon in the calorimeter: 1 positron per bunch, 1,000,000 bunches at 5 MeV, pencil beam. Note the maximum energy exceeding 5 MeV due to in-flight annihilation.

$\langle E_{Anni} \rangle$	Error	$\langle E_{NoAnni} \rangle$	Error	Fig
8.6	$2.6{\times}10^{-1}$	5.2	$2.2{\times}10^{-1}$	5

Table 3: comparison of mean energy for 1000 bunches of incoming positrons with 1000 e^+ per bunch. Energies and erros in MeV

2.3 Contribution to Mean Energy from Annihilation

Bremsstrahlung and annihilation processes inside the reconversion target produce most of the photons detected in the calorimeter. The contribution of annihilation to the mean energy of the emerging photons is considerable, as can be seen when disabling the latter in Geant4.

The numbers in Table 3 were obtained from Gaussian fits on the interpolated calorimeter, i.e. the sum of all crystals, for incident positrons at 5 MeV; 1000 per bunch, 1000 bunches with an iron core. As a result, I found that the mean energy is a factor of about $0.65 \approx \frac{2}{3}$ higher, when annihilation is present. This is an interesting result and good to know.

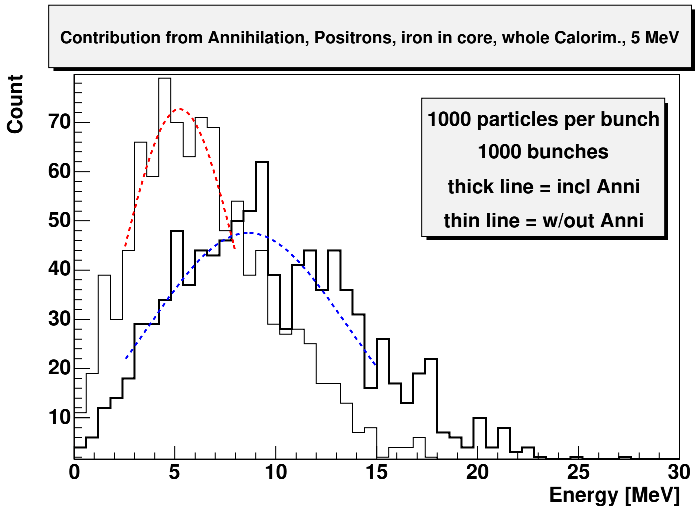

Figure 5: Shows the amplification of the mean energy due to annihilation at 5 MeV, 1000 positrons per bunch, 1000 bunches, Iron core.

2.4 Different Behavior for e^+ and e^-

Is there a difference in energy from Bremsstrahlung between positrons and electrons? The energy-loss due to Bremsstrahlung in matter is often considered to give equal amounts of radiation for electrons and positrons. This is correct for high energies of the order of hundreds of MeV or higher. However, as was shown by Kim et. al in 1986 [3], there are non-negligible differences for electrons and positrons at lower energies. Therefore, a Z-dependent correction is needed for the energy-loss inside the reconversion target. Keeping this in mind, I would like to compare the scaling factor calculated with known values from equations 6 to 7 to the one calculated from simulated values.
In our case the RT was made of Tungsten which has $Z = 74$. The scaling function η is proportional to $\frac{T}{Z^2}$, where T is the kinetic energy and Z the atomic number.
With

$$x = \log(7.52 \times 10^6 \frac{T}{Z^2}) \approx 1.93 \tag{6}$$

and the approximation

ppb	bnchs	$\langle E_{e^+} \rangle$	Error	$\langle E_{e^-} \rangle$	Error	η
1	10000	3.5×10^{-1}	7.0×10^{-2}	3.8×10^{-1}	5.2×10^{-2}	0.92 ± 0.32
100	1000	4.7	1.8×10^{-1}	5.7	1.7×10^{-1}	0.82 ± 0.22
1000	1000	5.4×10^{1}	4.4×10^{-1}	6.6×10^{1}	4.8×10^{-1}	0.82 ± 0.013

Table 4: Comparison of mean photon energy due to Bremsstrahlung at different statistics for positrons and electrons with Vacuum inside the core of the analyzing magnet when annihilation is not present. All energies in MeV.

ppb	bnchs	$\langle E_{e^+} \rangle$	Error	$\langle E_{e^-} \rangle$	Error	η
100	1000	6.5×10^{-1}	1.8×10^{-1}	6.7×10^{-1}	1.4×10^{-1}	0.97 ± 0.49
1000	1000	5.6	1.7×10^{-1}	7.6	1.6×10^{-1}	0.74 ± 0.04

Table 5: Comparison of mean photon energy due to Bremsstrahlung for positrons and electrons with iron in the core of the analyzing magnet when annihilation is not present. All energies in MeV.

$$\eta = 1/2 + (1/\pi)\arctan(0.42x + 0.0021x^3 + 0.00054x^5) \tag{7}$$

valid for $-8 < x < 9$, I found

$$\eta = 0.721.$$

These calculations were done following the Geant4 manual [2], section III.8.2.1. 'Cross Section and Energy Loss'.
Comparison of the difference in energy in the whole calorimeter for incident electrons and positrons, without contributions from annihilation - as was needed to see the desired effect - yielded the results available in Tables 4 and 5.
By dividing $\frac{\langle E_{e^+} \rangle}{\langle E_{e^-} \rangle} = \eta$, I calculated the scaling function for the simulated values. The difference between these and the one calculated according to the manual is rather large. It is interesting that the numbers match within the error range for an iron core, but not for a vacuum core. Yet, an in-depth study of the origin of these effects was not conducted. The intention here was to show that there are non-negligible differences in the energy-loss from Bremsstrahlung in matter between positrons and electrons. Figure 5 illustrates this.

Note on Statistics It is evident that high statistics were indispensable for my work. For the following simulations I used very high statistics using

ppb	bnchs	$\langle E_{e+} \rangle$	Error	$\langle E_{e-} \rangle$	Error
1	10000	4.2×10^{-1}	2.7×10^{-2}	4.6×10^{-1}	2.4×10^{-2}
100	1000	6.5	2.1×10^{-1}	6.3	1.6×10^{-1}
1000	1000	8.2×10^{1}	4.1×10^{-1}	6.9×10^{1}	3.4×10^{-1}

Table 6: Mean energies detected in the calorimeter for positrons and electrons for a vacuum core in the analyzing magnet. All energies in MeV.

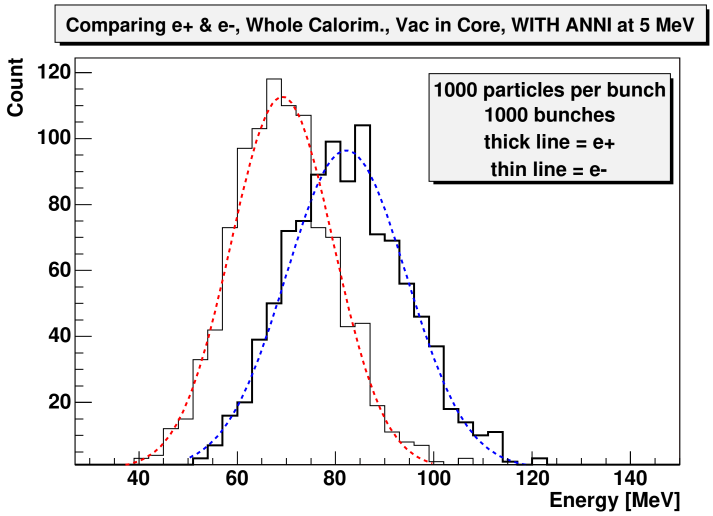

Figure 6: The interpolated crystal, 1000 particles per bunch, 1000 bunches at 5 MeV. Core-material: Vacuum. Annihilation processes present. Note the much higher mean energy for positrons

the computer farm for computation.
In the part of my work described in this section, I gained an overview and an understanding of the Geant4-based simulation and of some of the physical processes present. Good references for this topic include the online Geant4 manual [2], the online Root manual [4] and the NIST website [5].

3 Programs used for Analysis

3.1 Root

A great part of my work was to obtain an understanding of how to use the software I was working with. After that, I started to send large-scale simulations to the computer farm and to look to the data obtained from them. In order to do this, I had to become familiar with the basics of

ROOT, since I used it for the graphical and analytical analysis of the data. Later, I wrote some scripts, which, when run in ROOT, will do the following:

- WriteMacroFiles.C : Produces 26 macros for use in the simulations sent to the computer farm. 13 different energies with two polarization directions each. Includes gun direction, gun position, particle polarization, beam energy, number of bunches, number of particles per bunch, etc.

- WriteMegaTable.C : Produces a large ASCII table which includes all the important data from a farm-job. It sorts the asymmetries including errors and the mean energies for both directions of polarizations including errors by energy and crystal number of the calorimeter.

- CalcMegaTable.C : Reads out and plots the data from the large ASCII table in ROOT. This is in order to be able to see e.g. the shift in asymmetry due to shifting the beam on the reconversion target.

- A_x_pencil_5MeV.C : Plots the asymmetries over the offset for 6 different distances to the center of the RT for a pencil beam at 5 MeV.

- calc_Big_pencil.C : Plots the centered big beam and the centered pencil beam as a functions of beam energy. Produces both a plot for the mean energies and one for the asymmetries.

These files were produced in order to automize the process of calculating the analyzing power. Their goal is to reduce redundant steps and eliminate error sources in the code.

3.2 Geant4

Since the simulation program I was working with, the E166polarimeter program, is a Geant4 program, I had to become familiar with the structure of a program in Geant4 as well. Geant4 is a C++-based MonteCarlo simulation used for multiple purposes, one of which particle detector simulations is one of the most important ones. However, Geant4 is rather complex. Therefore, the extent of my work was limited to changing some details in the simulation, such as the beam shape, for example.
It should be mentioned here, that for my analysis, it was important to have polarized processes present in the Geant4 framework. These parts of the code are still in the development phase. During the course of my work, this implementation of polarization was gradually enhanced and updated. Therefore, my work can also be considered a cross-check of the validity of the Geant4 polarization processes. In fact, some problems did occur and helped to point out processes that still had to be worked on by the developers.

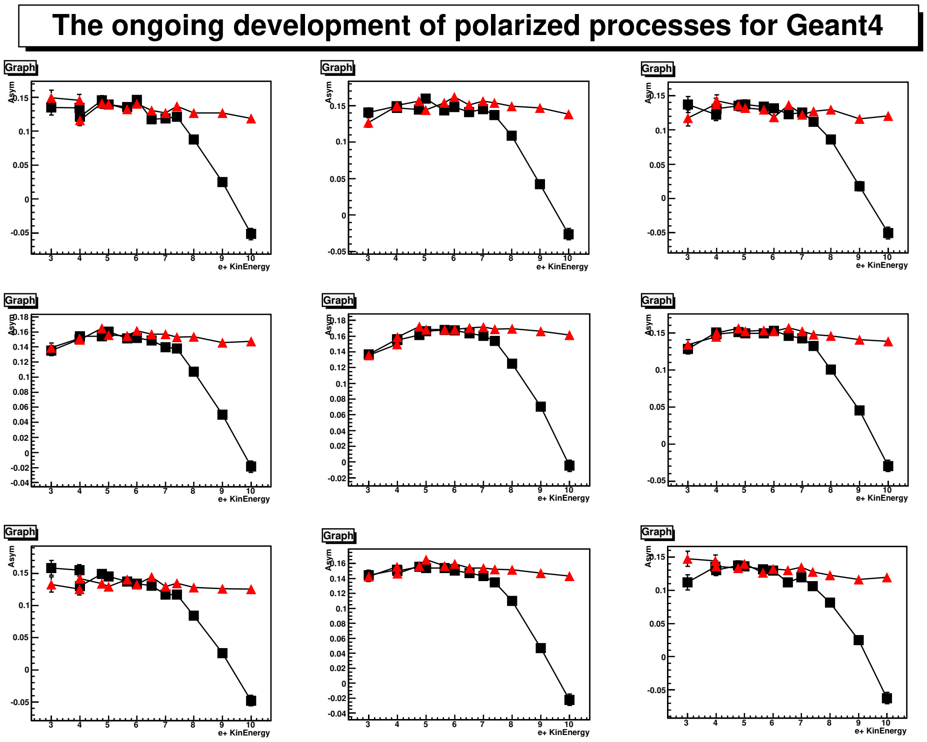

Figure 7: Shows the asymmetry as a function of kinetic positron energy. Note the drastic difference for energies above $\backsim 7MeV$ in the case of a pencil beam in the center of the RT before, indicated by black squares, and after, marked by red triangles, correcting a sign-error in Geant4. The drop-off line with the black quadratic markers indicated the mistake.

3.3 The E166 Polarimeter Program

The E166polarimeter program was really the heart of my work. The analyzing power had to be determined from simulations run with this code, written by Karim Laihem. Whenever I refer to changing the code of the simulation, e.g. the material inside the analyzing magnet, I am refering to changing the source files of this program.

4 Polarized Processes

As explained in the introduction, the goal of my work was to find the analyzing power of the positron polarimeter. Since the degree of polarization of the photons emerging from the reconversion target (RT) translates to the degree of polarization of the incident positron beam, this is an important task.
In this section, I will describe the simulations performed in order to determine the analyzing power, starting with a simplified picture and advancing to the realistic scenario, and the results obtained and conclusions that were drawn from them.
After creating the polarized positron beam, it is important to find its degree of polarization. Before the experimentally measured data can be analyzed, simulations for the analyzing power are needed. Once the energy-dependent analyzing power is known, it can be used to calculate P_γ according to to the explanation in part I and equation 1. In my simulations, P_γ and P_e were set to 100%. In this case, the asymmetry equals the analyzing power and does not need to be calculated separately. This procedure, of course, is a simplification, but it is useful, since the asymmetries are larger and their behavior for different energies and offsets from the center of the reconversion target can be better understood and simulated faster. From there, I wanted to continue to more quantitative simulations.

4.1 Pencil Beam

For first investigations of the behavior of the analyzing power a pencil beam in the center and at some offsets was simulated, starting from the center of the RT and taking small steps to a maximum displacement of 2.4cm - almost the edge of the RT which has a radius of 2.5cm. Due to the late discovery of the sign error in the Geant4 code mentioned in section 3.2, the asymmetries calculated for energies above $\backsim 7MeV$ are not to be used. Yet, for energies below this limit, as can be seen from Figure 7, it is possible to perform the desired analysis.

Figure 8 offers some very important conclusions. At first sight, one can see that the asymmetry drops rapidly in the left column of crystals as the pencil beam approaches the edge of the target, whereas it increases slightly for the right-most crystals.
This is a geometrical effect, since the scattered photons inside the iron have random directions. Photons that are scattered away from the system's z-axis are more vulnerable to the limited angular acceptance of the setup. This means that the closer the beam is to the lead ring around the iron core, the more radiation will be absorbed by it. The asymmetry approaches zero for the greatest offsets in the left-most crystals, since almost no energy could be detected by the CsI in this case.

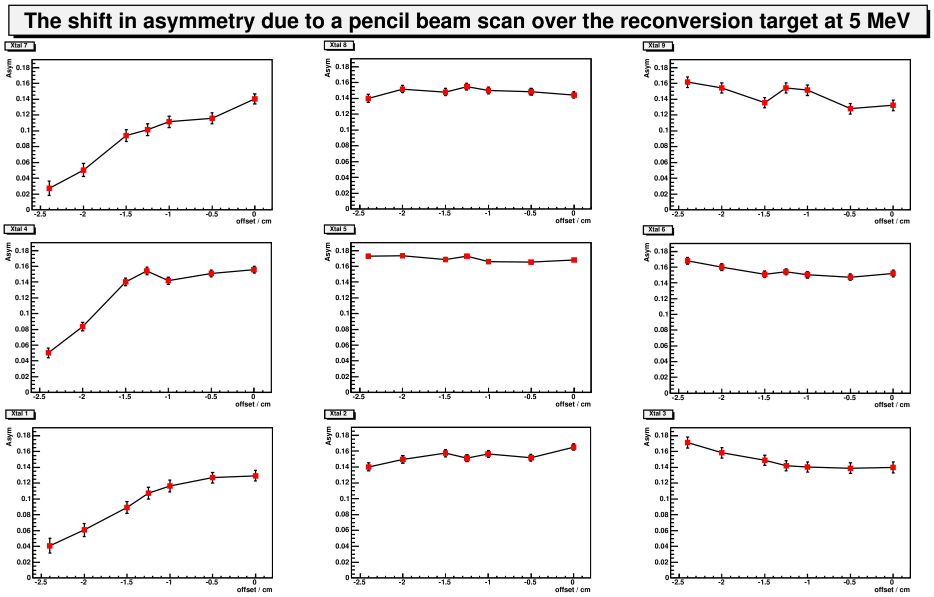

Figure 8: Asymmetry vs. offset on RT. Note the change in asymmetry which results from shifting the pencil beam along the x-direction of the RT at 5 MeV beam energy. Simulations were conducted for offsets of 0.0, 0.5, 1.0, 1.25, 1.5, 2.0 and 2.4 cm (from right to left, negative x-values). The datapoints for the center of the RT and for 1.25 cm were recalculated after fixing the sign-error mentioned in section 3.2. Since the sign error does not have a considerable effect on the asymmetry at 5 MeV, comparing the others as well was acceptible.

For the central crystal we can see a rather constant asymmetry. With the iron core covering all of the central crystal, this result is in accordance to expectations and provides an indication for the validity of the simulation on the one hand, and an argument for using the central crystal as the most important one for the experiment on the other.
The geometrical symmetry of the calorimeter suggests a symmetric distribution of the asymmetries in the crystals. Three groups of crystals can be distinguished. Crystals 1,3,7 and 9 form group 1, No.'s 2,4,6 and 8 constitute group 2; crystal 5 makes up for group 3. The behavior of the asymmetry for crystals within a group should be similar. Only crystal 8 deviates outside the error range, compared the other members of group 2. This may be due to statistical effects. The symmetry of the picture becomes clear when examining the smoothness of the asymmetry-lines. In the corner crystals, i.e. group 1, these lines are very bumpy, the side-crystals, i.e. group 2, they are much smoother.
For the right column of crystals, i.e. No.'s 3,6 and 9, the asymmetries are

slightly increasing. This can be seen best for No. 3, the kink in the line for crystal 9 can be misleading. The points are within the error ranges and can therefore be considered acceptible.

4.2 Broad Beam

In the beginning, it was planned to additionally run simulations for more realistic cases than pencil beams. The actual shape of the beam, according to the results from the experiment itself, covered the left half of the reconversion target.
Approaching this case, simulations were performed with a circular beam of 1cm radius as intermediate step. For this "broad beam" I used very high statistics. Similar to the above approach, I wanted to consider the following cases:

1. Beam in the center
2. At an offset of 1.25cm
3. Centered with an angle $\alpha \approx 0.29°$
4. 1.25cm off-center from an angle α

Of all the simulations I ran, only the first yielded good results, since Geant4 returned "segmentation faults" afterwards. These lead to zero-asymmetries, which could not be explained or resolved. Since we could not find the generators of the problems, no analysis of the more realistic beam scenarios could be performed. From the mean energies plotted in Figure 9, one can see that the mean energies of the two polarization directions for the second run of the broad beam in the center are virtually equal. This problem put an unfortunate end to my simulations.

During the course of writing this report, I found a possible candidate as a source for the error. Before the sementation faults started to occur, I simulated a randomly distributed beam in a circular area. This is how I obtained the data for the big beam in the center, which I am comparing to a pencil beam above, cf. Figure 10.
The beam shape was defined in Geant4 to be within a square of 2cm side length. An if-condition made sure that only events which were obeyed $x^2 + y^2 \leq R^2$, i.e. the ones inside a circle, were kept. In this way, less events were stored than had been started by the macro. For instance, for a macro which should have sent 5000 bunches, only about 3900 events were stored. In order to change this, a for-loop was introduced which made sure that the simulation would keep going, until the number of events matched the number of bunches sent. Ever since this change had been made, no asymmetries could be found anymore. Therefore, I conclude that there is a

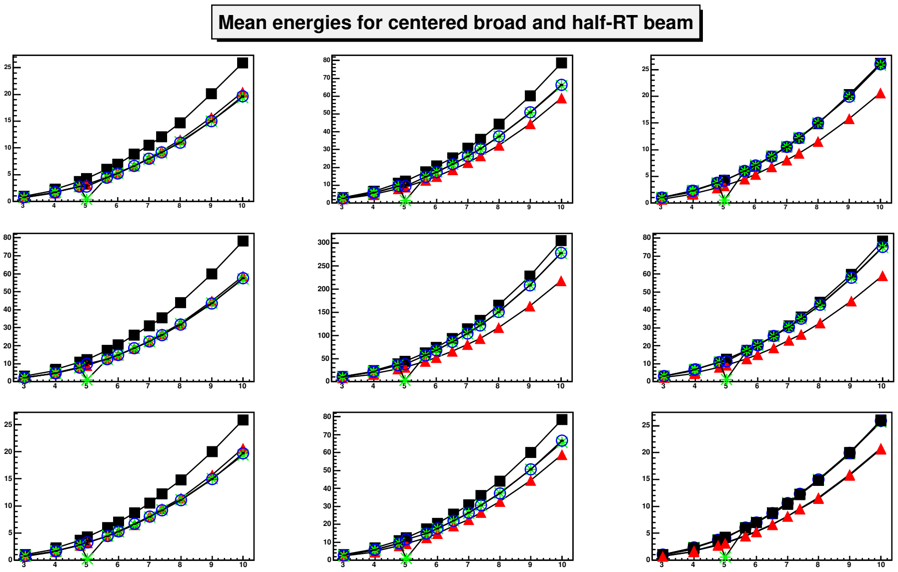

Figure 9: Mean energies in MeV over incident particle beam energy for broad beams in the center of the RT in MeV. The black squares and red triangles are values from earlier simulations, cf. Figure 10. The two markers lying on top of each other in each crystal illustrate the lack of asymmetry for the erroneous simulation runs.

clash between the number of bunches defined in the beginning and Geant4 trying to enforce the same number of events and thus sending more bunches than originally wanted by the macro.
A possible way of eliminating this error while keeping up higher statistics would be to increase statistics, i.e. the number of bunches sent, by a factor Δ, where $\Delta = \dfrac{A_{a^2}}{A_{\pi(\frac{a}{2})^2}}$. By this procedure, the possible clash could be avoided.
Unfortunately, the search for this error had to be postponed due to the approaching end of the Summer Student Program.

As mentioned before, data from the first run for a big beam was taken before the error started to occur. I used the data from this simulation for a consistency comparison with the centered pencil beam, cf. Figure 10.
How should we interpret this picture and what conclusions can we draw from it?
For crystal No. 5, the central one, the asymmetries coincide rather well. For energies above 4 MeV it seems as if it stayed rather constant between 16.5 % and 17.5 %. It almost looks as if in the higher-energy end it were

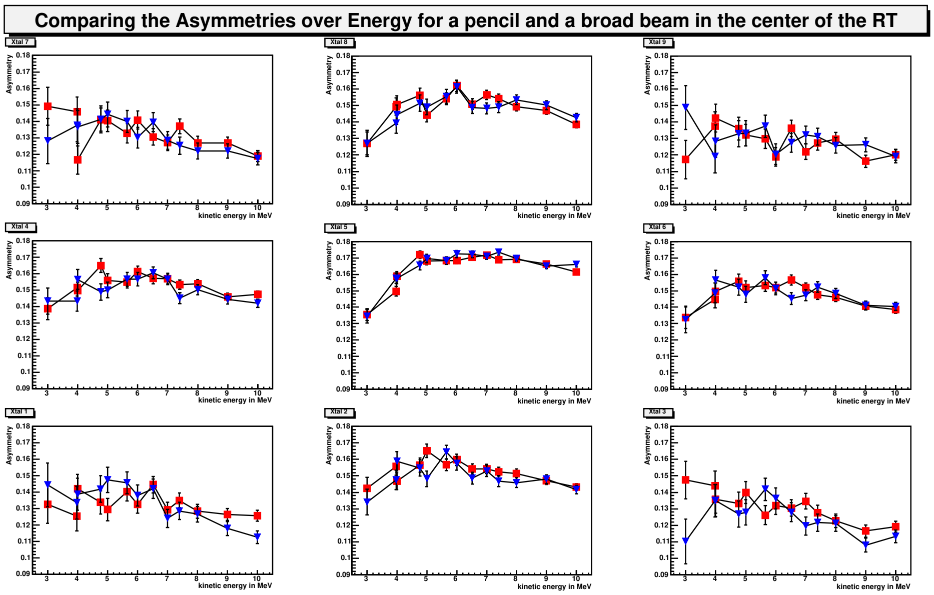

Figure 10: Illustrates the asymmetries over the incident beam energies for both a pencil beam (red squares) and a broad beam (blue triangles) in the center of the RT.

decreasing again. This behavior can be observed for the other crystals as well.
In the corner-crystals, the values deviate rather much from each other, especially at lower energies. The clearest example for this is the top left crystal, No. 7. Not only is there a large difference between the pencil and the broad beam, but also within the asymmetries for the pencil beam itself. Even though the neighboring energies are 3.98 MeV, 4 MeV and 4.77 MeV, the deviation for the 4 MeV data point is clearly outside the error range. This fact and the rather instable behavior for the other corner crystals may point to difficulties in simulating the asymmetries in these crystals. Since the transmission coefficient for a solid is energy-dependent and since the geometry of the calorimeter leads to only few detected events in the corner-crystals, even higher statistics, especially for the lower end of the energy spectrum simulated, would be needed to smoothen out these asymmetries. Obviously, not even the simulated 5,000 bunches of 10,000 positrons each were enough to do so here.
The crystals of group 2 show a nicer behavior. The asymmetries for the pencil and the broad beam are on top of each other within the error-range, with only few exceptions. An increase of asymmetry below 5 MeV is observed, with a slight decrease above maybe 6 or 7 MeV. The plots do not contain enough data points to really investigate this issue. The plot for crystal 5

shows qualitatively the same behavior, yet much clearer, and illustrates that a pencil beam constitutes a rather good first approximation.
At low beam energies, the errors are much higher than at higher energies. This results from a higher probability of absoption of radiation inside the iron core and the lower energy of the photons produced in the reconversion target.

4.3 Conclusion for the Analyzing Power

Although technical difficulties made it impossible to evaluate data for more realistic scenarios, the comparison of the asymmetries for the broad and the pencil beam yield the important information that in the central crystal, the analyzing power - for 100% polarized iron and positrons - remains rather constant around *0.165 - 0.175.* This value can be seen as a first estimate of the upper level of the analyzing power.
Yet, there remains great deals of work to be done.

5 What's Next?

The most important thing to do next would be to find the source of the segmentation fault. As soon as this is eliminated, one can proceed to simulations approaching the realistic scenario. These include:

- Simulating the beam shapes desired in Part 4.2, especially the case of a beam illuminating half of the reconversion target
- Gradually decreasing the polarization of the iron core to around 7% in order to see the effect on A_γ
- Calculating P_γ for $P_e \approx 7\%$ and compare it with the degree of polarization measured for the photons in the photon polarimeter
- Tabulating the values for the analyzing power and cross-checking with the asymmetries measured in the experiment

Part III
Acknowledgements and References

6 Acknowledgements

I would like to thank my supervisors Karim Laihem, Andreas Schälicke and Sabine Riemann for their great support and advice and DESY, DESY Zeuthen in particular, for offering this opportunity to students.
Figures 1 and 2 courtesy of Karim Laihem.

My deepest gratitude to my family for their never-ending help and incredible support.

References

[1] The E166 Proposal available at
http://www.slac.stanford.edu/pubs/slactns/slac-tn-04-018.html

[2] The Geant4 Online Physics Reference Manual available at
http://geant4.web.cern.ch/geant4/G4UsersDocuments/UsersGuides/PhysicsReferenceManual/html/PhysicsReferenceManual.html

[3] L. Kim et al. Phys. Rev. A33 (1986) 3002.

[4] The Root Online Manual available at
http://root.cern.ch/root/doc/RootDoc.html

[5] The website of the National Institute of Standards and Technology
http://www.nist.gov/